# Dynamic modelling and linear quadratic Gaussian control of a twin-rotor multi-input multi-output system

**S M Ahmad**[1], **A J Chipperfield**[2] and **M O Tokhi**[3]*
[1]Department of Mechanical and Marine Engineering, University of Plymouth, UK
[2]School of Engineering Sciences, University of Southampton, UK
[3]Department of Automatic Control and Systems Engineering, University of Sheffield, UK

**Abstract:** This paper presents an investigation into the modelling and control of a one-degree-of-freedom (1 DOF) twin-rotor multi-input multi-output (MIMO) system (TRMS). The behaviour of the TRMS in certain aspects resembles that of a helicopter. Hence, it is an interesting identification and control problem. A dynamic model characterizing the TRMS in hover is extracted using a black-box system identification technique. The extracted model is employed in the design of a feedback linear quadratic Gaussian compensator, namely the stability augmentation system (SAS). This has a good tracking capability but requires high control effort and has inadequate authority over residual vibration of the system. These problems are resolved by further augmenting the system with a command path prefilter, resulting in the command and stability augmentation system (CSAS). The combined feedforward and feedback compensator satisfies the performance objectives and obeys the actuator constraint. The control law is implemented in realtime on the TRMS platform.

**Keywords:** command and stability augmentation, feedforward control, helicopter, linear identification, linear quadratic Gaussian, stability augmentation, twin-rotor multi-input multi-output system

## NOTATION

| | |
|---|---|
| ARMAX | autoregressive moving average with exogenous input model |
| **A, B, C, D** | constant real system matrices of appropriate dimension |
| BSF | band-stop filter |
| CF | centre frequency |
| CSAS | command and stability augmentation system |
| $C(s)$ | command path filter |
| d.c. | direct current |
| DOF | degree of freedom |
| $F_1, F_2$ | thrust generated by the rotors in the vertical and horizontal planes |
| $G(s)$ | plant transfer function |
| $H(s)$ | controller transfer function |
| **I** | identity matrix |
| **J** | cost function to be minimized |
| **K** | optimal feedback controller gain matrix |
| LPF | low-pass filter |
| LQG | linear quadratic Gaussian |
| LQR | linear quadratic regulator |
| $\mathbf{L}_C$ | observer gain matrix |
| MIMO | multi-input multi-output |
| PRBS | pseudorandom binary sequence |
| PSD | power spectral density |
| **P** | solution to the Riccati equation |
| $q, r$ | individual elements of matrices **Q** and **R** respectively |
| **Q, R** | states and control weighting |
| $\mathbf{Q}_e, \mathbf{R}_e$ | process and measurement noise weighting |
| *ref* | reference input |
| SAS | stability augmentation system |
| TRMS | twin-rotor multi-input multi-output system |
| $u(\cdot)$ | input to the main rotor (V) |
| UAV | unmanned air vehicle |
| $x$ | state vector |
| $y(\cdot)$ | output pitch angle (rad) |

*The MS was received on 23 September 2002 and was accepted after revision for publication on 24 January 2003.*
* *Corresponding author: Department of Automatic Control and Systems Engineering, University of Sheffield, Mappin Street, Sheffield, S1 3JD, UK.*



## 1 INTRODUCTION

Research interest in innovative, *new-generation* air vehicles such as unmanned air vehicles (UAVs), oblique-

wing aircraft configurations, tilt rotor, tilt wing, delta wing, canard control surfaces, X-wing and tilt body is rapidly growing. There is also a small but growing literature on laboratory platforms simulating complex aircraft manoeuvres [1–4]. The interest stems from the fact that such air vehicles are highly agile, stealthy, multipurpose and capable of executing different tasks such as surveillance, aerial mapping and inspection, which are beyond the domain of their *classical* counterparts. These features, however, are at the expense of more involved procedures for modelling and control design.

However, modelling details of these vehicles are not reported owing to the classified nature of such projects. Moreover, the flight mechanics equations are not always easy to establish from the first principles, i.e. using laws of physics, for non-standard aircraft configurations. Yet, these equations are imperative for designing and studying flight control systems. In most classical fixed- and rotary-wing aircraft, the role of system identification is to estimate the parameters of a linearized six-degree-of-freedom (6 DOF) equation of motion from flight or wind tunnel data. Here, the structure is known and the parameters of the model have some physical meaning and are often called stability and control derivatives. However, in the present study, which is concerned with the modelling and control of a laboratory helicopter, no model structure is assumed *a priori*. Such a *black-box modelling* approach yields input–output models with neither an *a priori* defined model structure nor specific parameter settings reflecting any physical aspects. The former approach has been reported in the modelling of a number of UAVs (see, for example, references [5] to [8]). However, this paper investigates the latter approach for modelling a class of modern air vehicles. The utility of this approach is demonstrated by employing a twin-rotor multi-input multi-output (MIMO) system (TRMS). The dynamics of the TRMS (see Fig. 1), in certain aspects, resembles that of a helicopter. The TRMS is a laboratory set-up designed for control experiments by Feedback Instruments Limited [9]. From the control point of view it exemplifies a high-order non-linear system with significant cross-coupling. The present investigation, however, is confined to 1 DOF modelling and control; 2 DOF TRMS modelling is reported in reference [10].

It is evident from the rig that structural vibrations occur owing to the presence of rotor load at the end of the cantilever beam and motor torque, inducing bending movement, while in operation. This vibration appears in the system response as oscillations with a long settling time. Therefore, the second part of this paper deals with the twin problem of vibration attenuation and command tracking. Thus, the goal of the second part is to develop methods to reduce motion and uneven mass induced vibrations in the TRMS during operation as well as to achieve reasonable command signal tracking capability. The assumption is that the motion and the rotor load are the main sources of system vibration. A practical way of controlling a system with resonant modes is to use a combination of feedback and feedforward control. This paper investigates a feedback control and combined feedforward and feedback control technique, referred to as the stability augmentation system (SAS) and the command and stability augmentation system (CSAS) respectively. In the present work, a linear quadratic Gaussian (LQG) compensator is used as a state feedback inner loop controller, and digital filters as a feedforward compensator. This combined approach is particularly widely employed in aircraft control design [11]. The approach requires that the natural resonant frequencies of the system be determined through suitable identification and modelling techniques.

The compensators are designed and simulated within the Simulink simulation environment. The compensators are then implemented on the rig using the real-time kernel, which provides a mechanism of real-time measurement and control of the TRMS in a WINDOWS environment. Finally, a comparative assessment of the performance of the control strategies within simulation and experimental studies is provided. Preliminary results of this work have been reported in reference [12].

## 2 EXPERIMENTAL SET-UP

A description of the experimental set-up of the TRMS is shown in Fig. 1. The TRMS consists of a beam pivoted on its base in such a way that it can rotate freely both in its horizontal and vertical planes. There are rotors (the main and tail rotors), driven by d.c. motors, at both ends of the beam. A counterbalance arm with a weight at its end is fixed to the beam at the pivot. The state of the beam is described by four process variables: horizontal and vertical angles measured by position sensors fitted at the pivot, and two corresponding angular velocities. Two additional state variables are the angular velocities of the rotors, measured by tachogenerators coupled to the driving d.c. motors.

In a typical helicopter, the aerodynamic force is controlled by changing the angle of attack of the blades. The laboratory set-up is constructed such that the angle of attack of its blades is fixed. The aerodynamic force is controlled by varying the speed of the motors. Therefore, the control inputs are supply voltages of the d.c. motors. A change in the voltage value results in a change in the rotational speed of the propeller, which results in a change in the corresponding angle of the beam [9]. In Fig. 1, $F_1$ and $F_2$ represent the thrust generated by the rotors in the vertical and horizontal planes respectively.

## 3 MODELLING OF THE TRMS

The objective of the identification experiments is to estimate a linear time-invariant (LTI) model of the 1 DOF

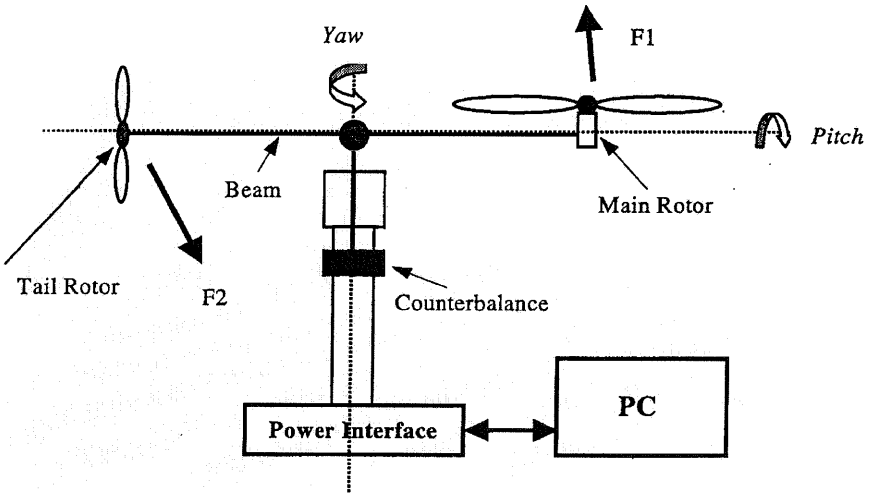


**Fig. 1** Twin-rotor MIMO system

TRMS in hover without any prior system knowledge pertaining to the exact mathematical model structure. The rig configuration is such that it permits open-loop system identification, unlike a helicopter which is open-loop unstable in hover mode. The system was excited with a pseudorandom binary sequence (PRBS) of different bandwidths (2–20 Hz) in order to ensure that all resonant modes of the system are captured both in the range of interest, i.e. 0–3 Hz, and, out of curiosity, to find out if any modes exist beyond this range. Finally, a PRBS of 5 Hz bandwidth and 60 s duration was deemed fit for this study. The PRBS magnitude was selected so that it does not drive the TRMS out of its linear operating range. Good excitation was achieved from 0 to 5 Hz, which includes all the important rigid body and flexible modes of the system.

This section discusses in brief the identification of the TRMS, which involves three steps: characterization, identification and verification. Further modelling details can be found in the authors' earlier work [**13**].

### 3.1 Mode or structure determination

Theoretically, the TRMS will have an infinite number of *normal modes* with associated frequencies. However, it is intuitively assumed that the main dynamics (*modes*) of the TRMS lie in the 0–1 Hz range. It is further assumed that the rotor dynamics are at significantly higher frequencies than the rigid body dynamics. Hence, this can be neglected, and the rotor influence is lumped into the rigid body derivatives. Under these broad hypotheses, system investigation is carried out to characterize the behaviour of the TRMS through a series of experiments. The power spectral density plot of the pitch response to the PRBS input signal, as shown in Fig. 2, indicates closely spaced modes between 0 and 1 Hz as expected, with a main resonant mode at 0.34 Hz which can be attributed to the main body dynamics. A model order of 2, 4 or 6 corresponding to prominent normal modes at 0.25, 0.34 and 0.46 Hz is thus anticipated [**13**].

### 3.2 Identification

The PRBS signal was used for excitation, and a multistep input, also referred to as 3-2-1-1 in aerospace literature, was used for validation. These signals, along with their corresponding outputs, are shown in Figs 3 and 4 respectively. A fourth-order autoregressive moving average with exogenous inputs (ARMAX) model was employed, which gave better representation of system dynamics, as can be seen in Fig. 5, implying inclusion of the main rotor influence in the model structure. Hence, subsequent investigations are based on the fourth-order ARMAX model, using the Matlab System Identification Toolbox [**14**]. Linear system identification is covered in a number of textbooks [**15**].

The Bode plots of the model are shown in Fig. 6. Both the gain and phase plots of the estimated model are in good agreement with those of the actual system, obtained from measured system input/output data. As noted, the model gives a reliable representation of the TRMS dynamics and, as will be shown next, has a high predictive capability.

### 3.3 Time-domain validation

*Verification*, which assesses the predictive quality of the extracted model, is a key final step in a system identification process. In this cross-validation study, the model is tested against a multistep input (3-2-1-1). A comparison of the simulated model output and the experimental

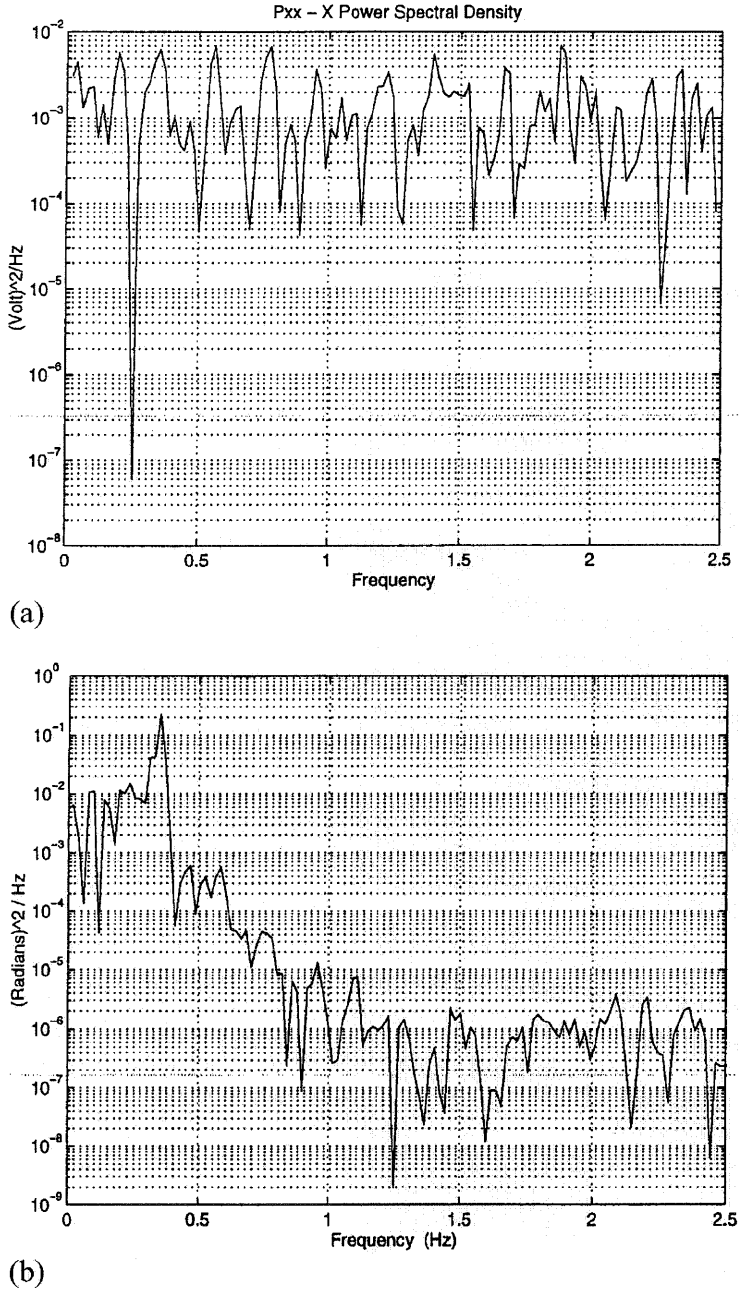


**Fig. 2** Power spectral density of (a) PRBS signal and (b) pitch response

output is shown in Fig. 5. Overall, the predictive capability of the model is quite good, especially considering the sensitive nature of the TRMS to ambient disturbances. Although there are still some discrepancies, the overall agreement is satisfactory. These discrepancies can be attributed to the mild oscillatory nature of the TRMS even in the steady state, as well as being very sensitive to the slightest atmospheric disturbance. The combined effect is reflected in these figures, with the occasional shooting of peaks as a result of slight wind, even when the input signals have ceased to exist. However, it is presumed that the resulting model is suitable for further control analysis. The parametric model is given in the next section.

## 4 CONTROL STRATEGY

Having successfully obtained a linear model for the pitch (vertical) plane, the second important issue is to design a suitable controller that is robust to modelling errors. This controller is expected to satisfy the desired performance specification. The performance objectives for this study consist of robust tracking of the commanded *pitch*

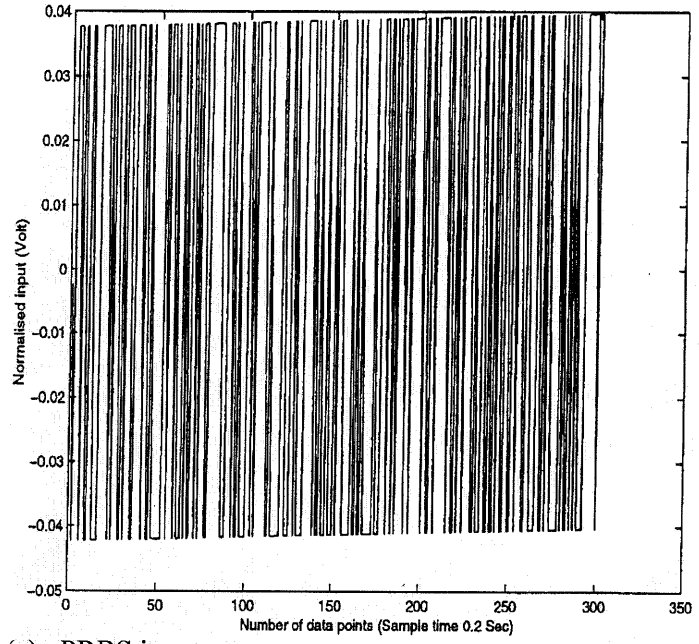


(a) PRBS input

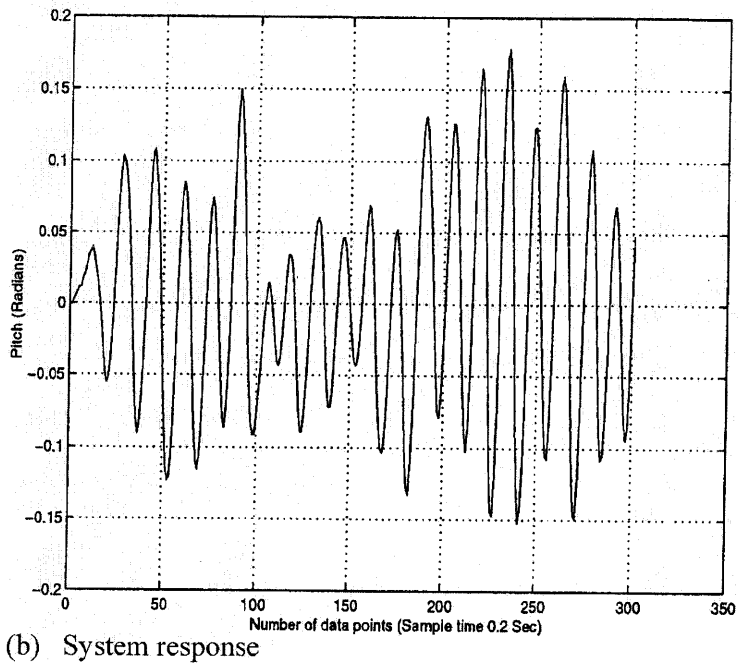


(b) System response

**Fig. 3** Input and output signals used for modelling

angle with low overshoot, a quick settling time of residual oscillations, good disturbance rejection capability and a high response bandwidth (i.e. short rise time) consistent with the dynamic capabilities of the TRMS airframe and available control energy. In this study, the LQG control paradigm is considered, as this ensures stability, exhibits robustness to system parameter variations and is also compatible with the MIMO control system design procedure. The TRMS operational condition is a flat horizontal boom, representing hover mode.

### 4.1 Problem definition

The presence of the main resonance mode at 0.34 Hz, evident from Fig. 2b, is the primary cause of vibration in the TRMS. The residual motion (vibration) is induced

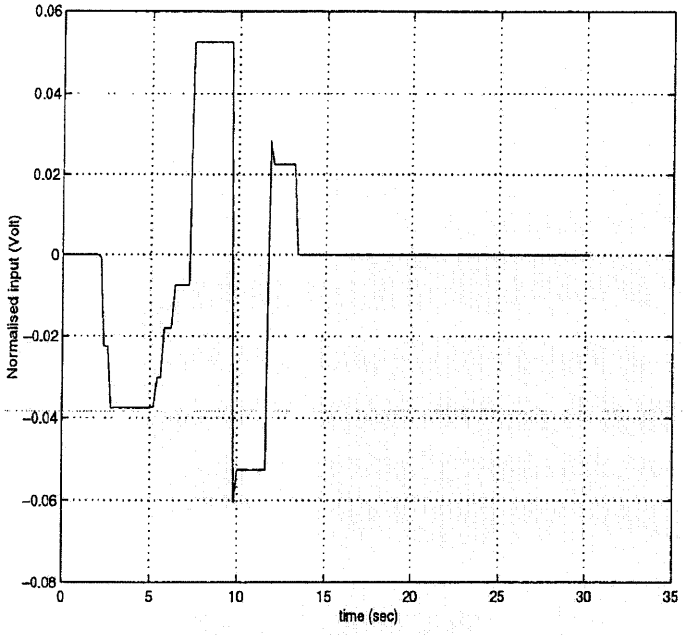


(a) Multistep input

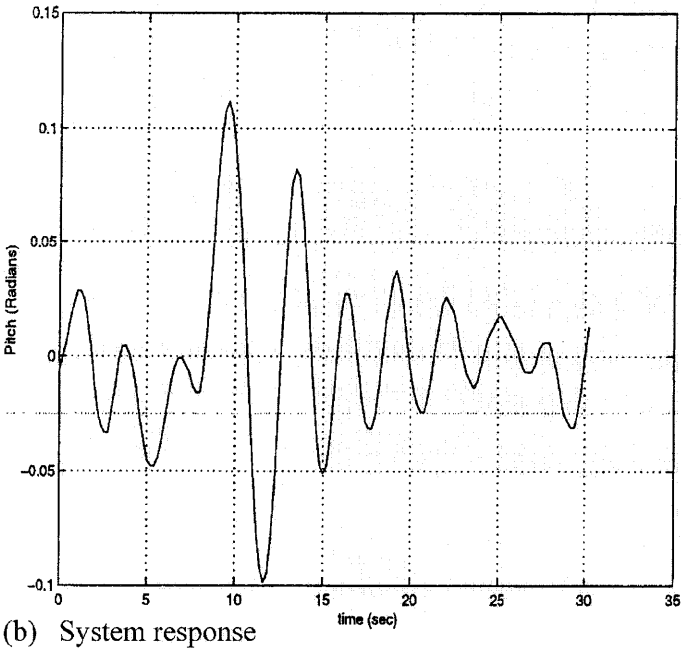


(b) System response

**Fig. 4** Input and output signals used for model cross-validation

in flexible structures primarily as a result of faster motion commands and, as mentioned in section 1, owing to the presence of rotor load at the two ends of the main beam. The occurrence of any vibration after the reference position has been reached will require additional settling time before the new manoeuvre can be initiated. Therefore, in order to achieve a fast system response to input command signals, it is imperative to reduce this vibration. This feature is desirable in any fast manoeuvring system, such as fighter aircraft. Various approaches have been proposed to reduce vibration in flexible systems. They can be broadly categorized as feedforward, feedback or a combination of feedforward and feedback methods. The latter is considered in this work.

### 4.2 The 1 DOF TRMS model

A 1 DOF model, i.e. the pitch (vertical) plane single-input single-output (SISO) model, is considered for controller design and implementation purpose. A discrete-time SISO transfer function model, obtained via

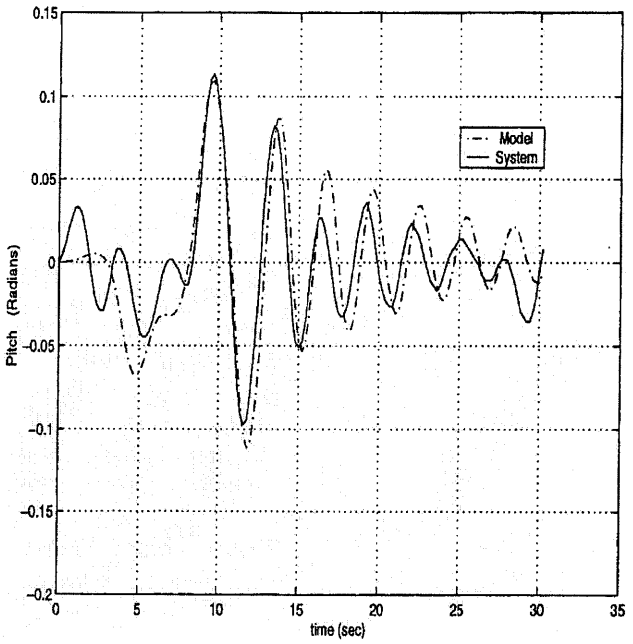


**Fig. 5** System and model response to a 3-2-1-1 input

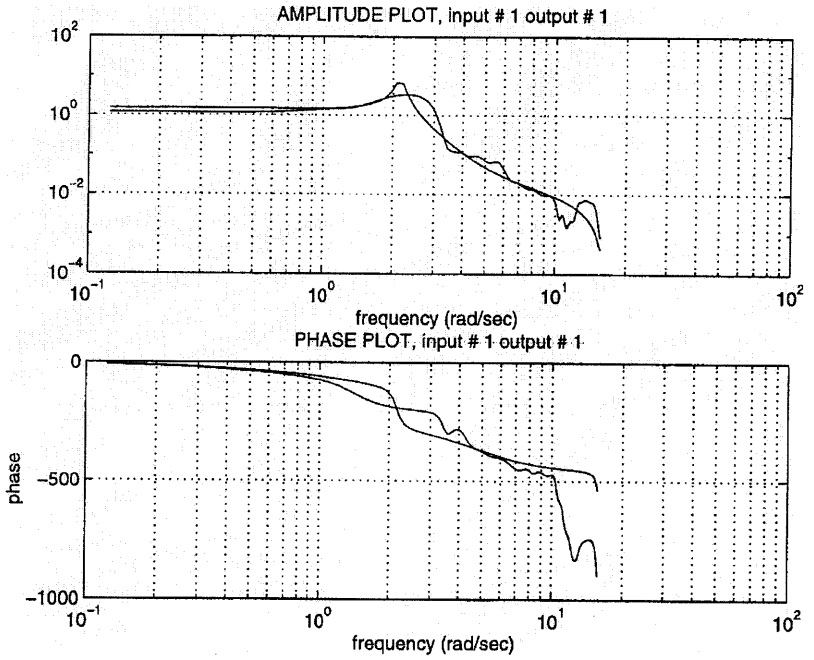


**Fig. 6** Bode plots of model (smooth) and actual system (non-smooth) characteristics

system identification of the previous section, is given as

$$\frac{y_1}{u_1} = \frac{(z-0.9805+1.3281i)(z-0.9805-1.3281i) \times (z+1.0743)}{(z-0.8926-0.4095i)(z-0.8926+0.4095i) \times (z-0.7541)(z-0.4685)} \quad (1)$$

where $y_1$ is the pitch angle (rad) and $u_1$ is the main rotor input (V). Note that the system is non-minimum phase with zeros outside the unit circle. The detrimental effect of this on the swiftness of response will be evident in the later section. The equivalent pitch plane state-space representation for the 1 DOF pitch plane model is then of the form

$$\boldsymbol{x}(k+1) = \mathbf{A}\boldsymbol{x}(k) + \mathbf{B}\boldsymbol{u}(k)$$
$$\boldsymbol{y}(k) = \mathbf{C}\boldsymbol{x}(k) + \mathbf{D}\boldsymbol{u}(k) \quad (2)$$

where **A**, **B**, **C** and **D** are system matrices of appropriate dimensions, given as

$$\mathbf{A} = \begin{bmatrix} 3.007 & 1.0 & 0 & 0 \\ -3.5 & 0 & 1.0 & 0 \\ 1.8096 & 0 & 0 & 1.0 \\ -0.341 & 0 & 0 & 0 \end{bmatrix}$$

$$\mathbf{B} = \begin{bmatrix} 0.0205 \\ -0.0278 \\ 0.0458 \\ -0.0033 \end{bmatrix}$$

$$\mathbf{C} = [1.0 \quad 0 \quad 0 \quad 0]$$

$$\mathbf{D} = [0.0097]$$

### 4.3 LQG regulator

LQG compensators are designed by solving two separate but *dual* problems, that is, the linear quadratic regulator (LQR) and optimal (Kalman) observer. The objective of the LQG is to minimize the average energy over all frequencies captured by the closed-loop transfer function from exogenous inputs to the error signal. The plant output error is augmented with an integrator to achieve zero steady state tracking error. The goal of LQR is to find the control sequence $\boldsymbol{u}(k)$ that minimizes the quadratic cost on the states and inputs:

$$\mathbf{J} = \frac{1}{2}\sum_{k=0}^{N} [\boldsymbol{x}^{\mathrm{T}}(k)\mathbf{Q}\boldsymbol{x}(k) + \boldsymbol{u}^{\mathrm{T}}(k)\mathbf{R}\boldsymbol{u}(k)] \tag{3}$$

where $\boldsymbol{x}$ is the augmented state vector including the state of the integrator, **R** is a positive scalar and yields a matrix of optimal gains **K** for the state feedback and **Q** is the weighting matrix on the states. The optimization of the cost function gives the optimal control signal as

$$\boldsymbol{u}(k) = -\mathbf{K}\boldsymbol{x}(k) \tag{4}$$

with

$$\mathbf{K} = [\mathbf{R} + \mathbf{B}^{\mathrm{T}}\mathbf{P}\mathbf{B}]^{-1}\mathbf{B}^{\mathrm{T}}\mathbf{P}\mathbf{A} \tag{5}$$

where $\mathbf{P} = \mathbf{P}^{\mathrm{T}} \geqslant 0$ is the unique positive-definite solution, found by solving the discrete matrix Riccati equation

$$\mathbf{P} = \mathbf{Q} + \mathbf{A}_a^{\mathrm{T}}\mathbf{P}\mathbf{A}_a - \mathbf{A}_a^{\mathrm{T}}\mathbf{P}\mathbf{B}_a(\mathbf{R} + \mathbf{B}_a^{\mathrm{T}}\mathbf{P}\mathbf{B}_a)^{-1}\mathbf{B}_a\mathbf{P}\mathbf{A}_a \tag{6}$$

The plant matrix $\mathbf{A}_a$ in the Riccati equation is an augmented matrix including the additional error state vector. This is equivalent to including integral action on the tracking error of the system as described earlier, and $\mathbf{B}_a$ is a suitably augmented control matrix. Furthermore, the plant model has four states, but only one state is measurable, necessitating the inclusion of an observer. The optimal observer design is the *dual* of the optimal regulator, and hence the observer gain matrix $\mathbf{L}_C$ is computed in a similar manner to the regulator, except that the observer gains are computed only for the plant states; i.e. integral error state is not included. It was ensured that the estimator roots were faster than the closed-loop control roots, so that the total system response was dominated by the control roots. This was achieved by choosing suitable standard covariance matrices $\mathbf{Q}_e$ and $\mathbf{R}_e$. The LQG compensator is obtained by combining the state feedback with the estimator, as shown in Fig. 7.

### 4.4 Controller design

The dynamic characteristics of the closed-loop system depend on the matrices $\mathbf{A}_a$ and $\mathbf{B}_a$, as well as the weighting matrices **Q** and **R**, and are quite complex. A pragmatic approach, therefore, is to choose a range of **Q** and **R** matrices, generate the corresponding regulator gain matrices **K** and subsequently simulate the closed-loop response. The gain matrix that satisfies the performance criteria is the appropriate one. Another rule is to define **Q** and **R** as

$$\mathbf{Q} = \mathrm{diag}(q_1, q_2, \ldots, q_n)$$

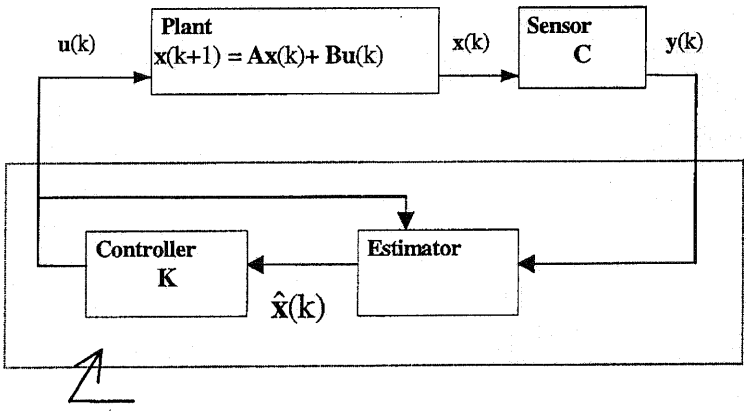


**Fig. 7** Schematic of combined estimator and controller

and

$$\mathbf{R} = \text{diag}(r_1, r_2, \ldots, r_n) > 0$$

and to use an initial estimate of $q_i$ and $r_i$ as [16]

$$q_i = \left[\frac{1}{(e_i)_{\max}}\right]^2 \quad \text{and} \quad r_i = \left[\frac{1}{(f_i)_{\max}}\right]^2 \tag{7}$$

where $e_i$ and $f_i$ are the values of the $i$th elements of the corresponding vectors, and subscript 'max' defines the maximum acceptable value. This approach implicitly trades between tracking and control energy performance. Further details of optimal control and the selection criteria for weighting matrices can be found in most standard textbooks [16, 17]. In the present study, various combinations of **Q** and **R** were investigated [18]. However, only the case of $\mathbf{Q} = \mathbf{I}$, $\mathbf{R} = 75$ is reported in this section, where **I** is the identity matrix. The choice of weighting matrices implies that the states are equally weighted and that the actuator signal is heavily penalized to ensure an overdamped response and control is 'cheap'.

The **Q** and **R** matrices are adjusted so as to obtain good disturbance rejection, high damping and a bandwidth that provides fast response without saturating the control. The corresponding covariance matrices for the observer are selected to ensure faster estimator roots.

## 5 LQG SIMULATION RESULTS

In order to test the controller, different simulations of the linear model of the TRMS were carried out with a square wave input. The controller performance was tested within the Simulink simulation environment. The structure of the controller is shown in Fig. 8, with $H(s)$ representing the LQG controller with integral action. The inner loop control is referred to as the stability augmentation system, the primary role of which is to maintain static and dynamic stability.

The tracking capability in following a square wave *pitch* angle command is shown in Fig. 9 along with the control effort. The performance of the LQG compensator for the nominal TRMS model is characterized by an overdamped response, a considerable rise time (3 s), little overshoot and a slow settling time (12 s). The control effort is found to be high and saturates the actuator limit, denoted by dashed lines.

It can be inferred from the above results that, although SAS provides dynamic stability, it has inadequate direct control over *response shaping*; i.e. SAS has no discernible mechanism to achieve the desired system response.

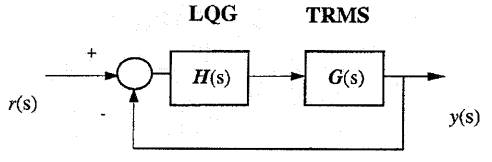


**Fig. 8** Stability augmentation system (SAS)

### 5.1 Command path prefilter

It is apparent that performance criteria such as speed of response or manoeuvrability and flying and handling qualities that are imposed on an aircraft/TRSMS are difficult to achieve entirely by *aerodynamic* means alone (i.e. using control surfaces in aircraft or rotors for the TRMS), while at the same time maintaining the dynamic stability of the airframe. This is particularly valid for highly agile, new-generation air vehicles, which are designed to operate over extended flight envelopes and aerodynamically difficult flight regimes. The TRMS performance can be further enhanced by employing *artificial non-aerodynamic* means. This, in essence, implies appending a command path prefilter or feedforward precompensator to the SAS. The new control structure, shown in Fig. 10, is referred to as the command and stability augmentation system.

The reference signal, $ref(s)$, is conditioned by a command control law, which determines the control and response characteristics of the augmented system. The consequence of this is *shaped response* and reduced control effort, which translate into reduced pilot workload and improved passenger comfort in the case of an aircraft.

Referring to Fig. 10, the overall closed-loop transfer function can be written as

$$\frac{y(s)}{ref(s)} = C(s)\left(\frac{H(s)G(s)}{1 + H(s)G(s)}\right) \tag{8}$$

It is important to note that the prefilter has no bearing on the stability, since it is outside the closed loop and does not appear in the characteristic equation (denominator) of the augmented plant.

The transfer function in equation (8) is that of the augmented TRMS and replaces that of the unaugmented TRMS, $G(s)$. Unmistakably, by judicious choice of $C(s)$ and $H(s)$, the control designer has considerable scope for achieving the desired stability, control and handling characteristics of the augmented system. The command prefilter $C(s)$ in this study comprises digital filters used for preprocessing the input to the TRMS, so that no energy is ever put into the system near its resonance. Thus, command input profiles that do not contain energy at system natural frequencies do not excite structural modes of vibration and hence require no additional settling time.

### 5.2 Prefilter results

To study the augmented system performance, a square wave is used, and the corresponding system response is measured. The main objective of this section is further

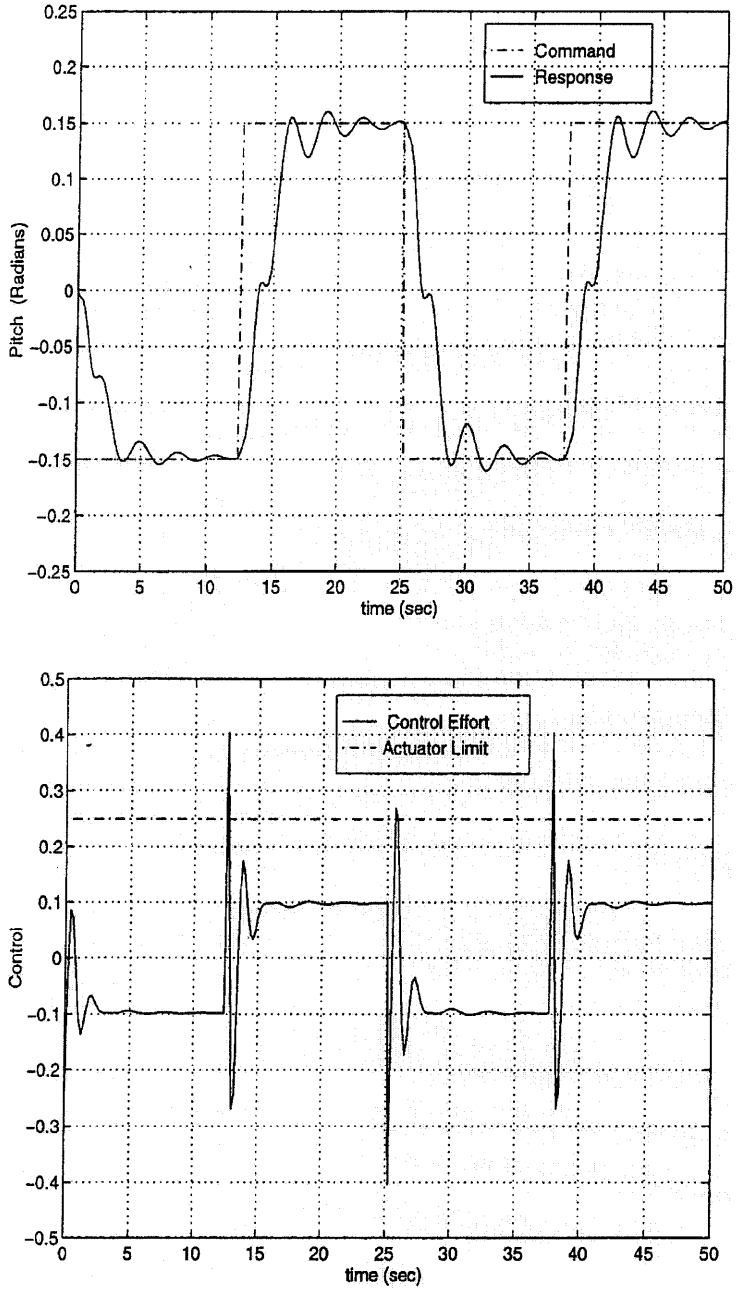


**Fig. 9** SAS response to square wave input, $\mathbf{Q} = \mathbf{I}$, $\mathbf{R} = 75$

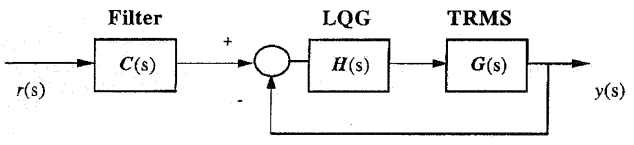


**Fig. 10** Command and stability augmentation system (CSAS)

to improve the augmented system performance by non-aerodynamic means. This is achieved by suppressing system vibrations at the first few dominant *resonance modes*. Two strategies, namely low-pass filtered and band-stop filtered input shaping, are used:

1. *Low-pass shaped input.* A second-order low-pass Butterworth filter (LPF) with a cut-off frequency at 0.2 Hz was designed and employed for processing the command input. The motive behind selecting the cut-off frequency at 0.2 Hz lies in the fact that the lowest mode of vibration of the system is found to be at 0.25 Hz. Hence, to attenuate resonance of the system, the cut-off frequency must be selected lower than the lowest mode of vibration. The corresponding system response to the low-pass filtered command square wave thus achieved is shown in Fig. 11, along with the corresponding control effort. Compared with Fig. 9, it is noted that the attenuation in the level of

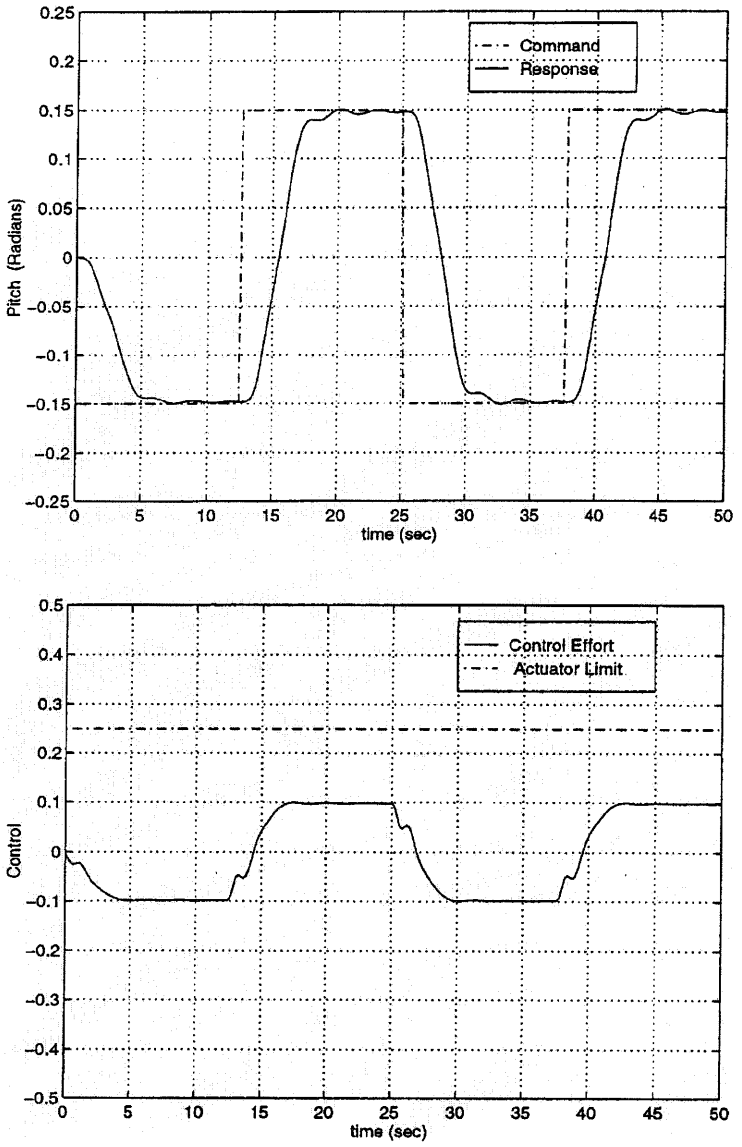


**Fig. 11** CSAS response using LPF (0.2 Hz cut-off), $\mathbf{Q} = \mathbf{I}$, $\mathbf{R} = 75$

vibration is significant with a quicker settling time (7–8 s). However, this is at the cost of a greater rise time (4.5 s).

The closed-loop system rise time characteristics can be further accentuated by allowing more 'energy' into the system. Therefore, the command prefilter with a cut-off frequency of 0.3 Hz is next investigated. The anticipated improvement in the rise time (3 s) is evident from Fig. 12, but this has led to degradation of the settling time (10 s). An important observation is that, after adding a command prefilter, the control is within the actuator limit and exhibits improved behaviour. This is a significant improvement over the feedback controller alone.

2. *Band-stop shaped input.* As above, a second-order digital Butterworth filter is used to study the CSAS performance with a band-stop shaped input. For effective suppression of vibration of the system, the centre frequency (CF) of the band-stop filter (BSF) has to be exactly at the same frequency or closer to the resonant modes. It was observed earlier (see Fig. 2) that the main resonant mode lies at 0.25 and 0.34 Hz, with additional clustered modes in close proximity to the main modes. Thus, band-stop filters with CFs of 0.25 and 0.34 Hz with a bandwidth of 0.2 Hz were selected. The resulting band-stop shaped square wave input was accordingly used, and the pitch response was measured. It is apparent from Fig. 13 that the control energy requirement is high and the response settling time is unacceptably large.

From the foregoing analysis it is deduced that the *command path* prefilter serves as a principal means of response shaping. Good response shaping characteristics

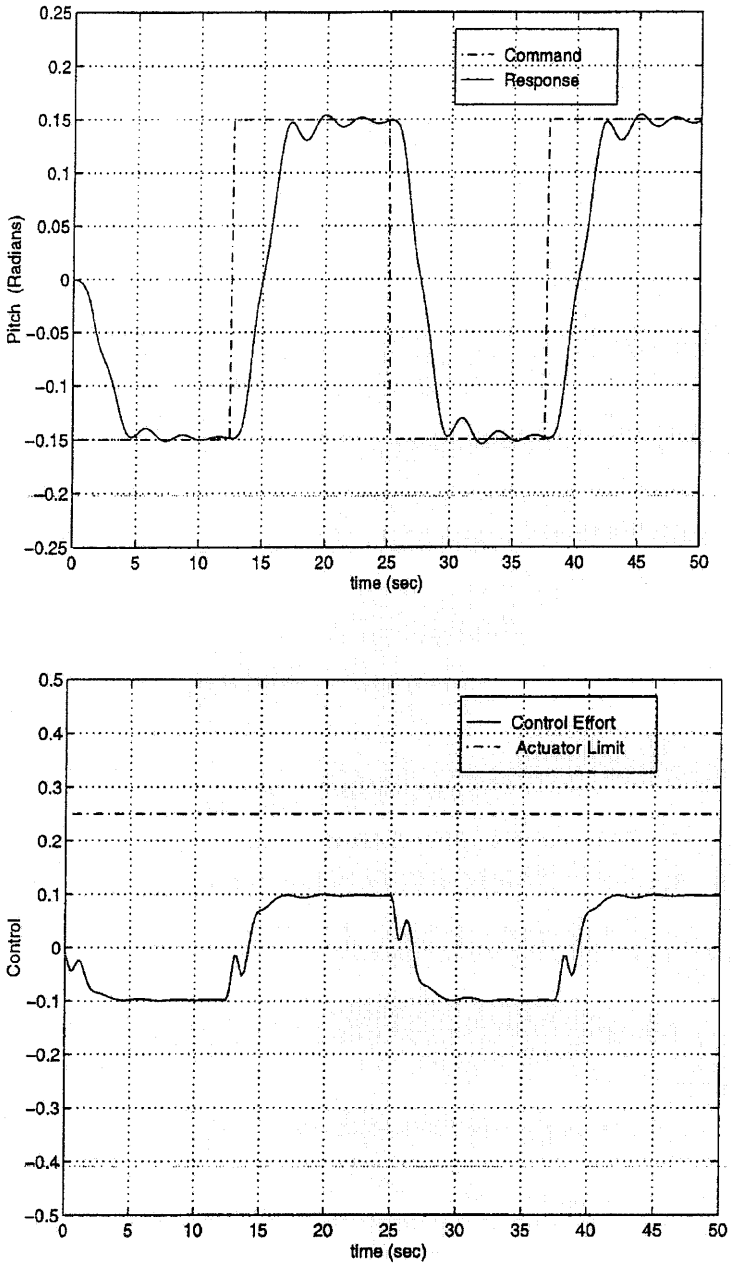


**Fig. 12** CSAS response using LPF (0.3 Hz cut-off), $\mathbf{Q} = \mathbf{I}$, $\mathbf{R} = 75$

are highly desirable in fast manoeuvring systems with rapidly changing command input.

## 6 CONTROLLER IMPLEMENTATION

In the previous section, various control schemes for controlling the TRMS were developed and tested within a simulation environment. The crucial test for any control paradigm is when implemented on a real system in the presence of real-world uncertainties and disturbances. The aim of this section is to apply these schemes to the TRMS. The TRMS hardware and software configuration is described in reference [9], and the control strategies are those developed in the previous section. It will be shown next, however, that the case investigated in the simulation environment is inadequate to achieve the desired closed-loop system performance. Therefore, an iterative process of controller design, simulation and implementation was carried out until desired system performance was obtained.

### 6.1 Controller implementation results

The controllers designed in the previous section were linked to the TRMS in real time through the

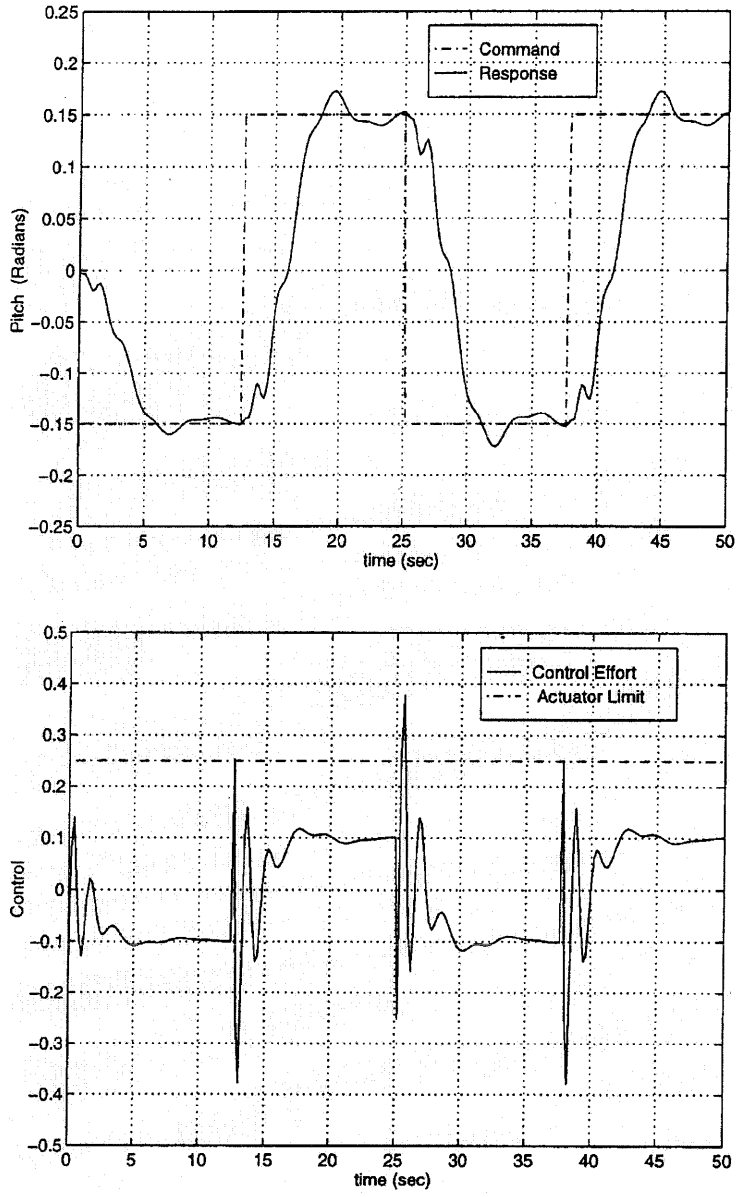


**Fig. 13** CSAS response using BSF (CF 0.25 and 0.34 Hz), $\mathbf{Q} = \mathbf{I}$, $\mathbf{R} = 75$

MATLAB–Simulink interface described in reference [9]. Both the SAS and the CSAS control schemes were executed. Essentially, the task of the LQG controller is to achieve robust tracking of command pitch angle by manipulating the input to the main rotor. The controlled output (pitch angle) is expected to have low overshoot, a quick settling time of residual oscillation and a reasonably fast speed of response without control saturation. Note that the operating point for this experiment is the flat horizontal main body, representing hover mode.

### 6.2 SAS implementation results

It is important to emphasize that the sampling time for modelling and control should be the same [15]. Hence, the sampling period is 5 Hz, i.e. the same as that used for modelling, and is set before the experiments. The steady state condition is allowed to be reached before injecting the square wave command input. The primary role of SAS is to ensure the stability of the system in the prescribed operating region.

*Case 1*: $\mathbf{Q} = \mathbf{I}$, $\mathbf{R} = 75$

The ability of the controller to track the reference square wave input and the control energy expended are shown in Fig. 14. Although the controller tracks the reference signal, the response is characterized by significant overshoot and erratic settling time. Poor control behaviour is also observed on the negative phase of the command cycle, which was absent in the simulations. The negative command essentially represents the downward motion

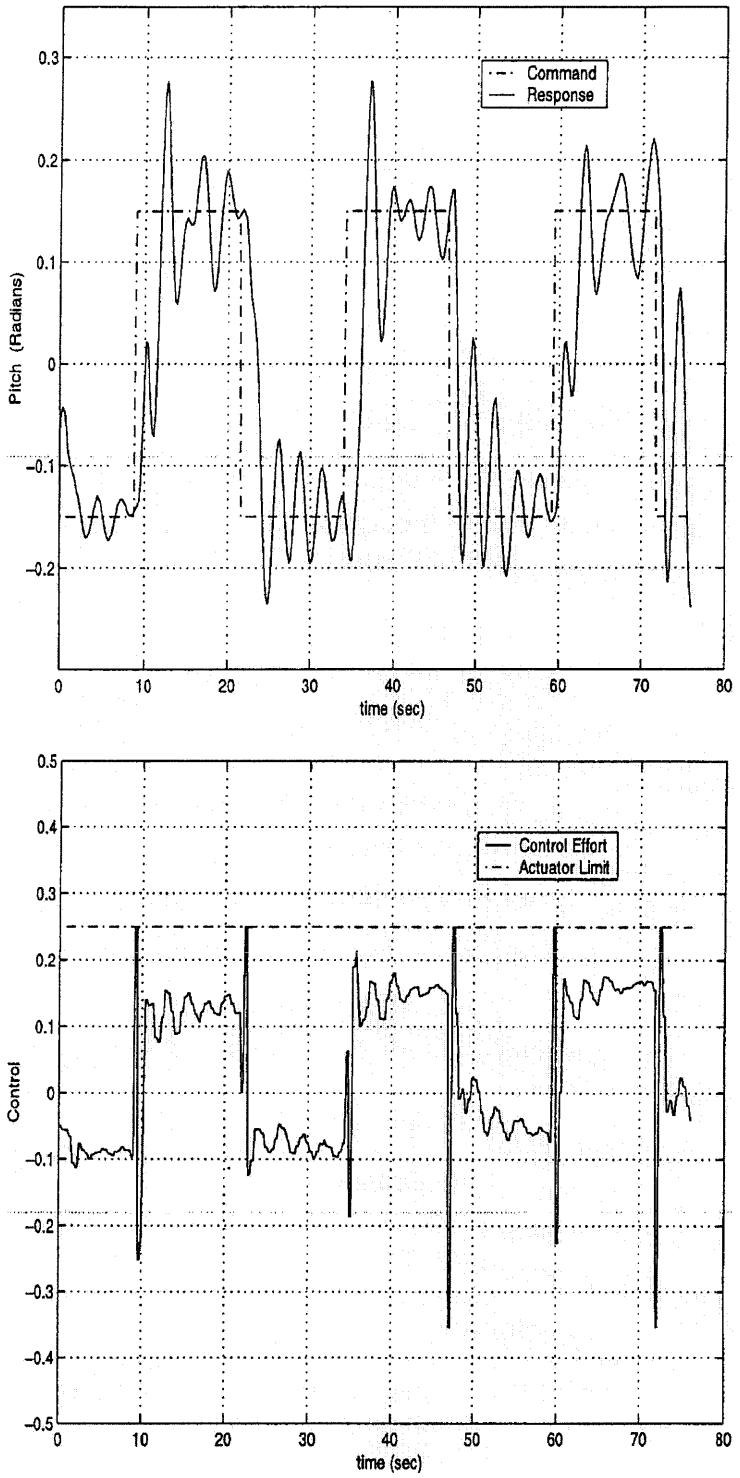


**Fig. 14** SAS response to square wave input, $\mathbf{Q} = \mathbf{I}$, $\mathbf{R} = 75$

of the main body. A sharp drop from the positive pitch angle, aided by gravity, exacerbates the inherent oscillatory nature of the TRMS. Without sufficient damping, control in this region is therefore poor. Similar to the simulation trials, the control saturates, but the system remains stable.

Since the case 1 SAS results are unsatisfactory, the trial and error procedure becomes apparent. Hence, two additional cases, namely case 2 ($\mathbf{Q} = \mathbf{I}$, $\mathbf{R} = 125$) and case 3 ($\mathbf{Q} = \mathbf{I}$, $\mathbf{R} = 100$), were investigated. The rationale for choosing these weights is to achieve further damped response, which is possible by penalizing the input. For

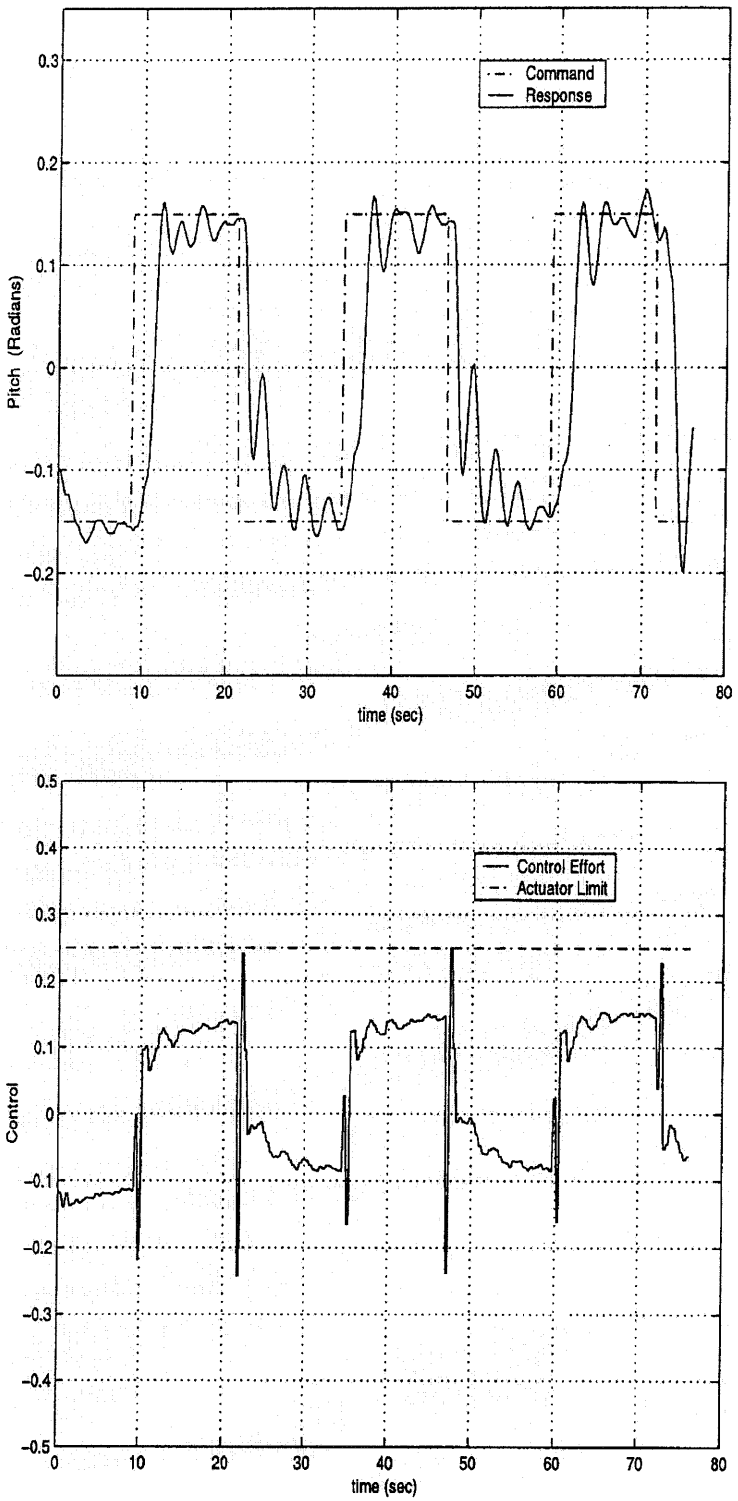


**Fig. 15** SAS response to square wave input, $\mathbf{Q} = \mathbf{I}$, $\mathbf{R} = 125$

conciseness, however, only the results of case 2 are reported here, and those of case 3 can be found in reference [**18**].

*Case 2*: $\mathbf{Q} = \mathbf{I}$, $\mathbf{R} = 125$

The TRMS response to the square wave reference signal is illustrated in Fig. 15. Much improved tracking is obtained on positive and negative cycles of the reference signal, implying good damping and hence tighter control. There is hardly any overshoot, with a smooth and acceptable settling time. Note that minor oscillations are due to inherent characteristics of the TRMS, which exhibits a minor oscillatory tendency even in the steady state condition. Thus, good settling behaviour is assumed. The

control signal is also within the saturation boundaries but operates very close to it.

In both case 1 and case 2 discussed above, the control demands are sharp, i.e. require a sudden burst of energy when the step command is applied. Such behaviour is undesirable, as it is detrimental to the plant operational life span. The jerky actuator movement will induce fatigue and thereby cause mechanical wear and tear of the TRMS.

### 6.3 CSAS implementation results

As explained in the simulation studies, improvement in the response characteristics of the augmented plant is sought by using the command path prefilter. In line with the simulation study, low-pass and band-stop filters are employed for input shaping.

#### *6.3.1 Low-pass shaped input*

Two second-order low-pass Butterworth filters with cut-off frequencies at 0.2 and 0.3 Hz were designed respectively and utilized for filtering the reference square wave input:

*Case 1*: $\mathbf{Q} = \mathbf{I}, \mathbf{R} = 75$

Figure 16 shows the TRMS pitch response to the 0.2 Hz filtered command signal. The input square wave is followed reasonably well with acceptable overshoot and response rise time, also displaying a good settling time characteristic. Control energy requirements are also minimal. Furthermore, a 0.3 Hz LPF is employed, which allows more input energy into the TRMS. The results are illustrated in Fig. 17. As anticipated, improved rise time behaviour is evident, but at the expense of larger overshoot and a longer settling time. No saturation of the actuator is noticed.

*Case 2*: $\mathbf{Q} = \mathbf{I}, \mathbf{R} = 125$

The system responses for this case are illustrated in Figs 18 and 19. Closer observation reveals a very similar pitch response to the reference signal and control pattern to case 1, with marginal differences. Like case 1, case 2 exhibits fairly good performance with low-pass filters of 0.2 Hz cut-off frequency. However, analogous to case 1, system performance deteriorates for case 2 with a command path prefilter of 0.3 Hz cut-off. The degradation in performance is due to the excitation of flexible modes in the 0–0.3 Hz bandwidth. This in turn induces oscillatory motion as can be seen in Fig. 19. In case 2, the actuator limits are not violated. A discernible feature of CSAS design with a low-pass filter is smooth actuator movements, unlike SAS, which causes sharp undesirable control movement.

#### *6.3.2 Band-stop shaped input*

From the simulations it is clear that the BSF does not yield acceptable results. Nevertheless, for completeness, its capability is examined. Analogous to LPF design, a second-order digital Butterworth filter was utilized to investigate the CSAS behaviour with a band-stop filtered square wave command input.

In this section, a BSF with a CF of 0.34 Hz and a bandwidth of 0.2 Hz is selected. Recall that 0.34 Hz corresponds to the main resonant mode of the TRMS. The responses for the two cases using this filter are depicted in Figs 20 and 21 respectively. The TRMS tracking capability for case 1 is poor, with high overshoot, a long settling time and inadequate control on the negative side of the reference trajectory. For case 2, the response is slightly better. In both cases, however, the control energy requirement is high. Sharp control movement is also noted in both cases, which again is unacceptable.

## 7 ROBUSTNESS TO DISTURBANCE

Robustness to external disturbance, such as wind gust, is also highly desirable for the TRMS application. The disturbance rejection capability of the controller is tested by applying a disturbance to the main body. The results are presented in Figs 22 and 23 for the two controllers. The disturbance was applied at around the 18–20 s interval, which is discernible by a sharp TRMS response from an early steady state condition. The moment the disturbing force is applied, the controller activity is increased, as can be seen from the control profiles of these plots. The controller rejects the applied disturbance and reverts back to its original equilibrium state.

## 8 DISCUSSION AND CONCLUSION

A 1 DOF SISO TRMS model, the dynamics of which resembles that of a helicopter, has been identified successfully. System identification has been shown to be an ideal tool to model non-standard aircraft configurations whose flight mechanics are not well understood. The extracted model has predicted the system behaviour well. A high-fidelity system model is an important first step in control system design and analyses. It has been revealed that the characteristic behaviour of the TRMS is of a non-minimum phase nature (plant with zero outside the unit circle). The speed of response to the input command for a non-minimum phase plant is limited by the existence of the non-minimum phase transmission zeros. Such a system has a slow speed of response, and this detrimental effect is discernible in both the simulation and the actual implementation results. Since minimum phase (plant with zeros within the unit circle)

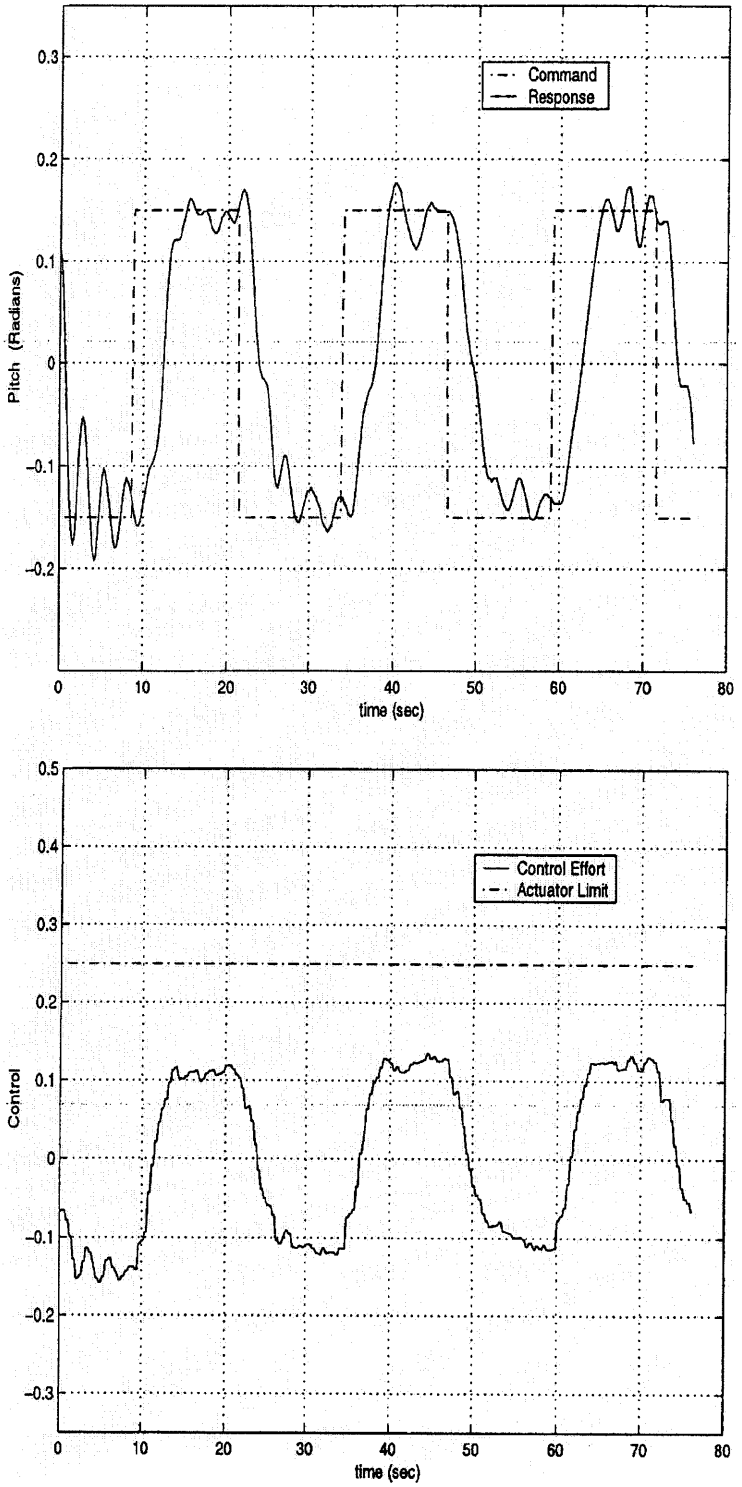


**Fig. 16** CSAS response using LPF (0.2 Hz cut-off), $\mathbf{Q} = \mathbf{I}$, $\mathbf{R} = 75$

airframes exhibit minimal response time, highly agile aircraft are augmented by including an additional control surface, called canard or 'flaperons', to the airframe [**19**]. A similar strategy could be adopted here or on any other platforms where such a feature is imperative.

This paper also investigated the design of an optimal control that stabilizes the TRMS and results in a good command tracking capability using aerodynamic means (i.e. using the main rotor), but at the cost of 'expensive' control. The performance of the feedback control has been improved by additionally using artificial non-aerodynamic means by employing a command prefilter.

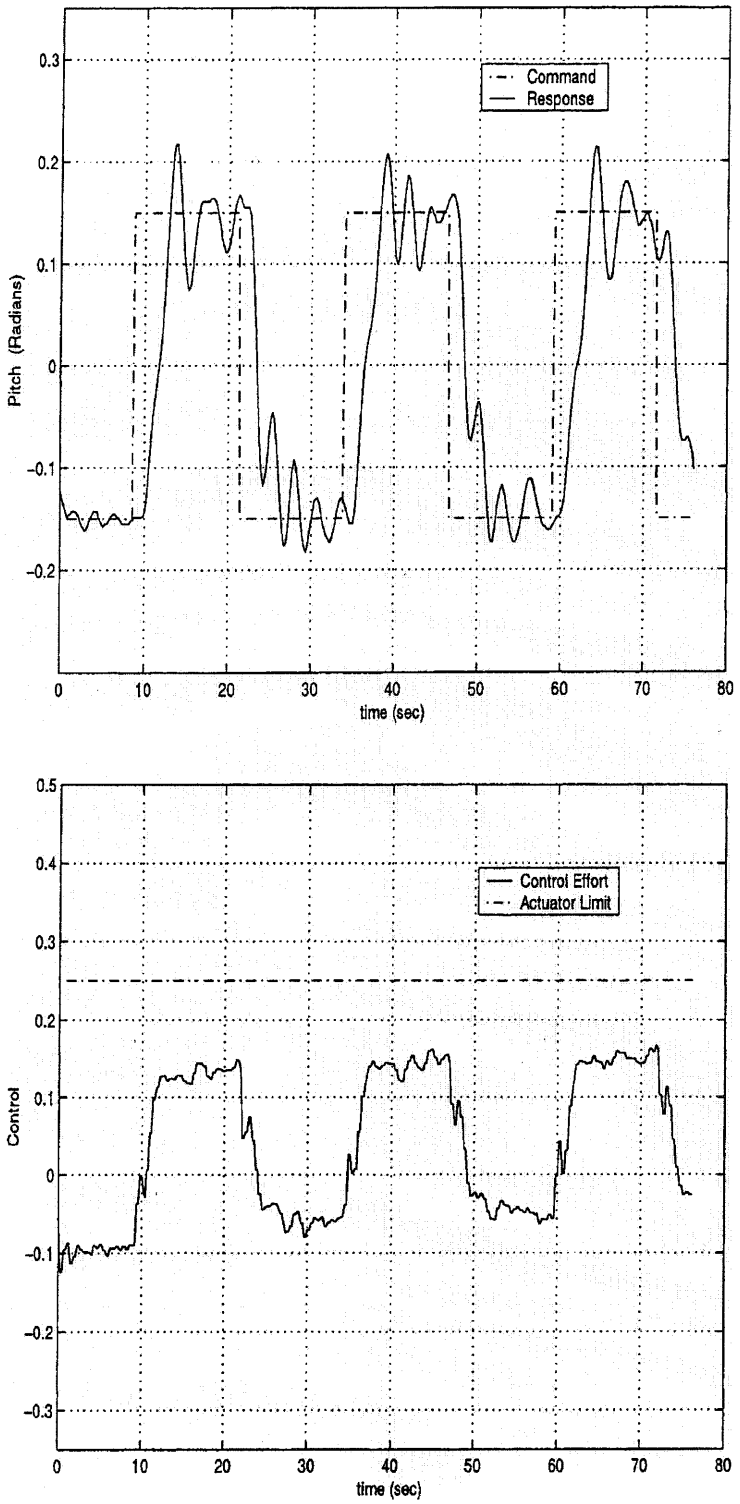


**Fig. 17** CSAS response using LPF (0.3 Hz cut-off), $\mathbf{Q} = \mathbf{I}$, $\mathbf{R} = 75$

The feedforward filter conditions the tracking command or set point so that system vibrations (oscillations) are reduced. Quick elimination of system vibrations is important for fast manoeuvring platforms, where the command signal changes rapidly. The advantage of this method is that it is not necessary to change the feedback control law in order to attenuate system vibration. The study revealed that better performance in attenuation of system vibration is achieved with a low-pass filtered command input, as compared with band-stop filtered inputs.

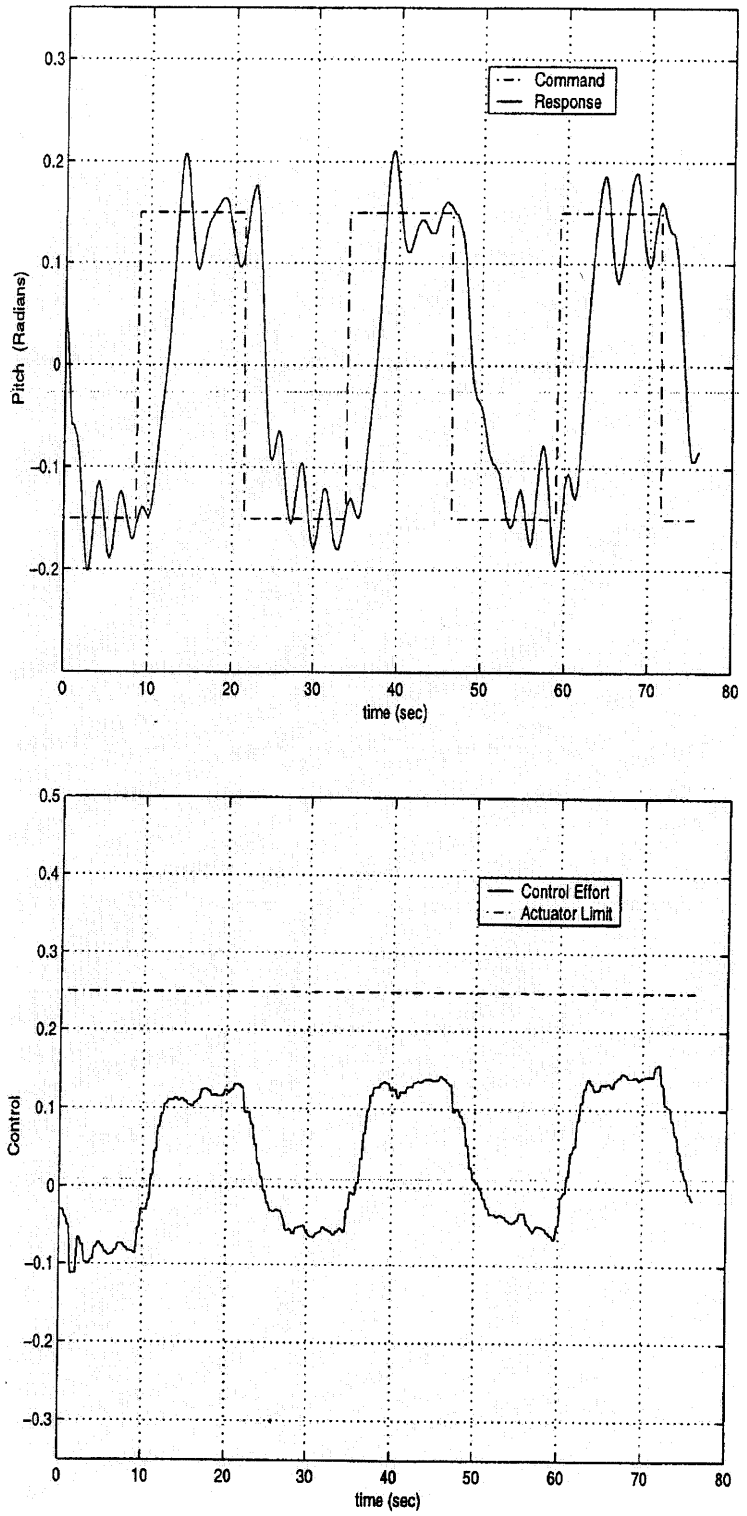


**Fig. 18** CSAS response using LPF (0.2 Hz cut-off), $\mathbf{Q} = \mathbf{I}$, $\mathbf{R} = 125$

This is due to indiscriminate spectral attenuation at frequencies above the filter cut-off frequency in the low-pass filtered input. However, this is at the expense of a slightly higher move time compared with a band-stop filter. With the command prefilter, the control effort is found to be within the actuator limits. Several different combinations of weighting matrices and command prefilter are imperative to achieve optimal performance. Thus, an appropriately designed feedforward and feedback controller is a practical approach to satisfy the

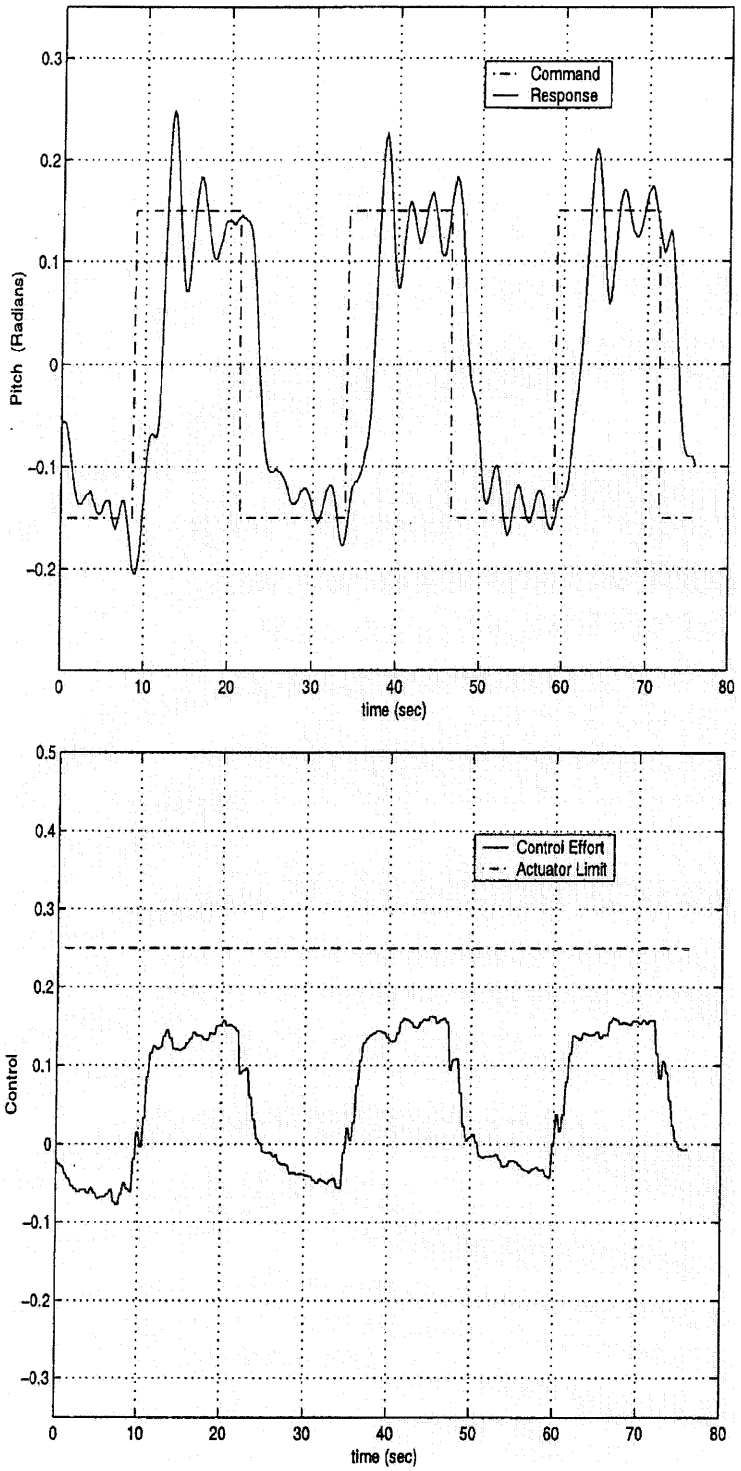


**Fig. 19** CSAS response using LPF (0.3 Hz cut-off), $\mathbf{Q} = \mathbf{I}$, $\mathbf{R} = 125$

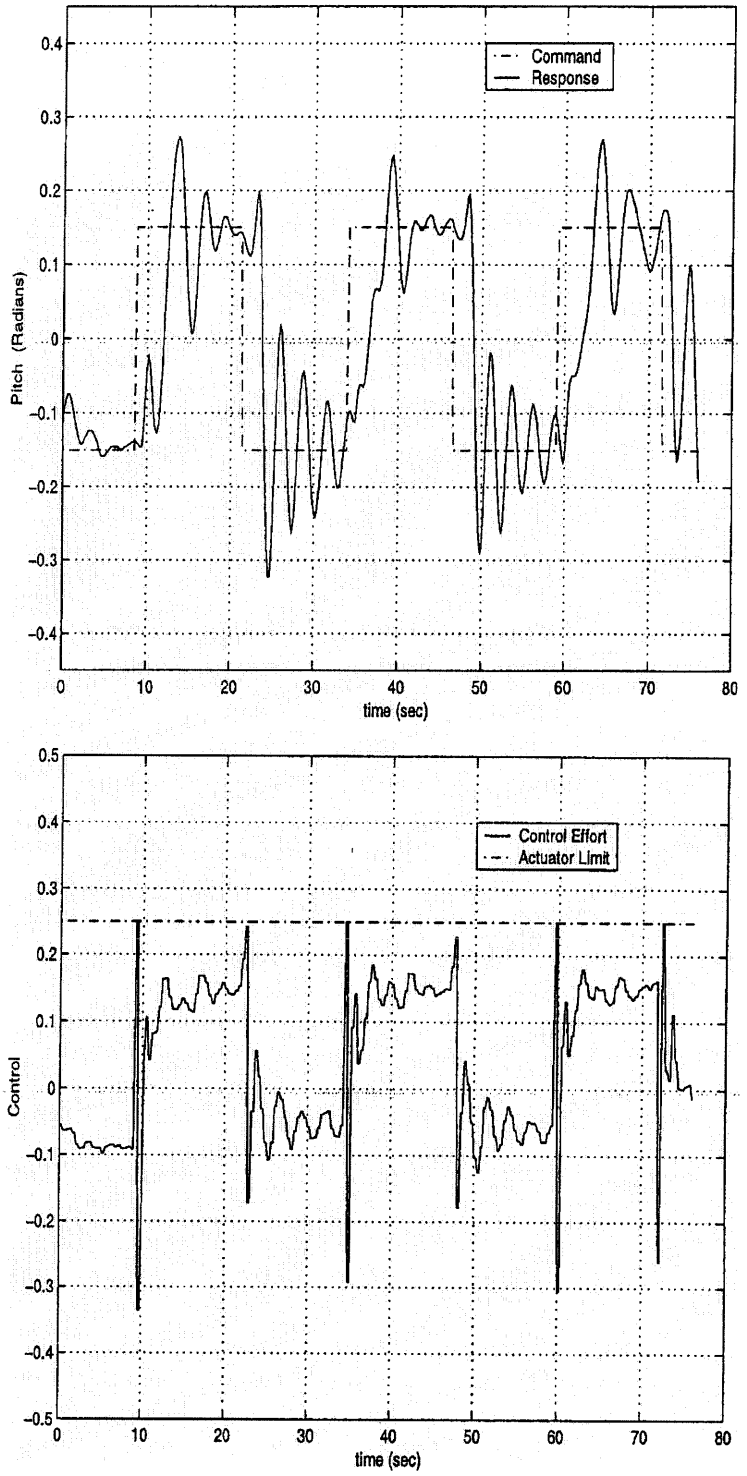


**Fig. 20** CSAS response using BSF (CF 0.34 Hz), $\mathbf{Q} = \mathbf{I}$, $\mathbf{R} = 75$

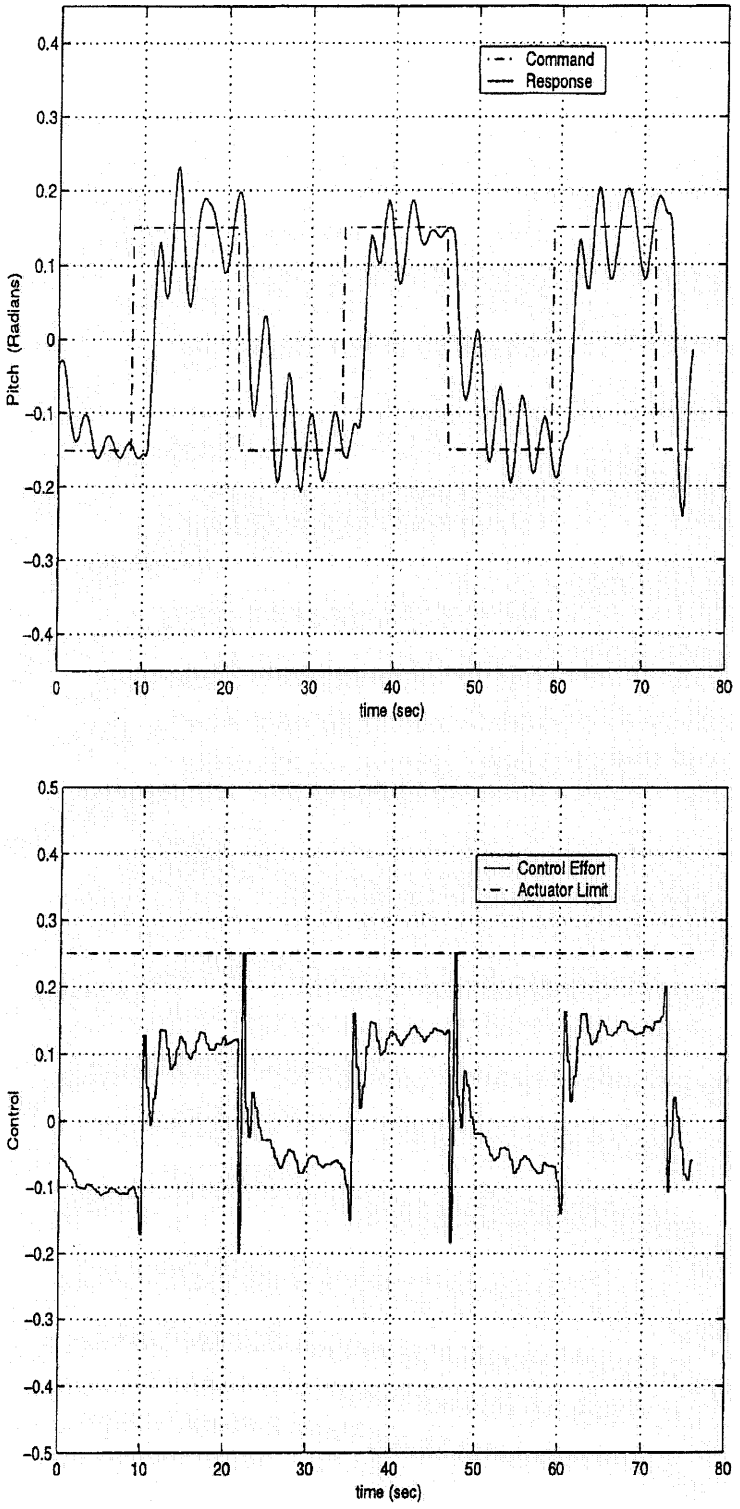


**Fig. 21** CSAS response using BSF (CF 0.34 Hz), $\mathbf{Q} = \mathbf{I}$, $\mathbf{R} = 125$

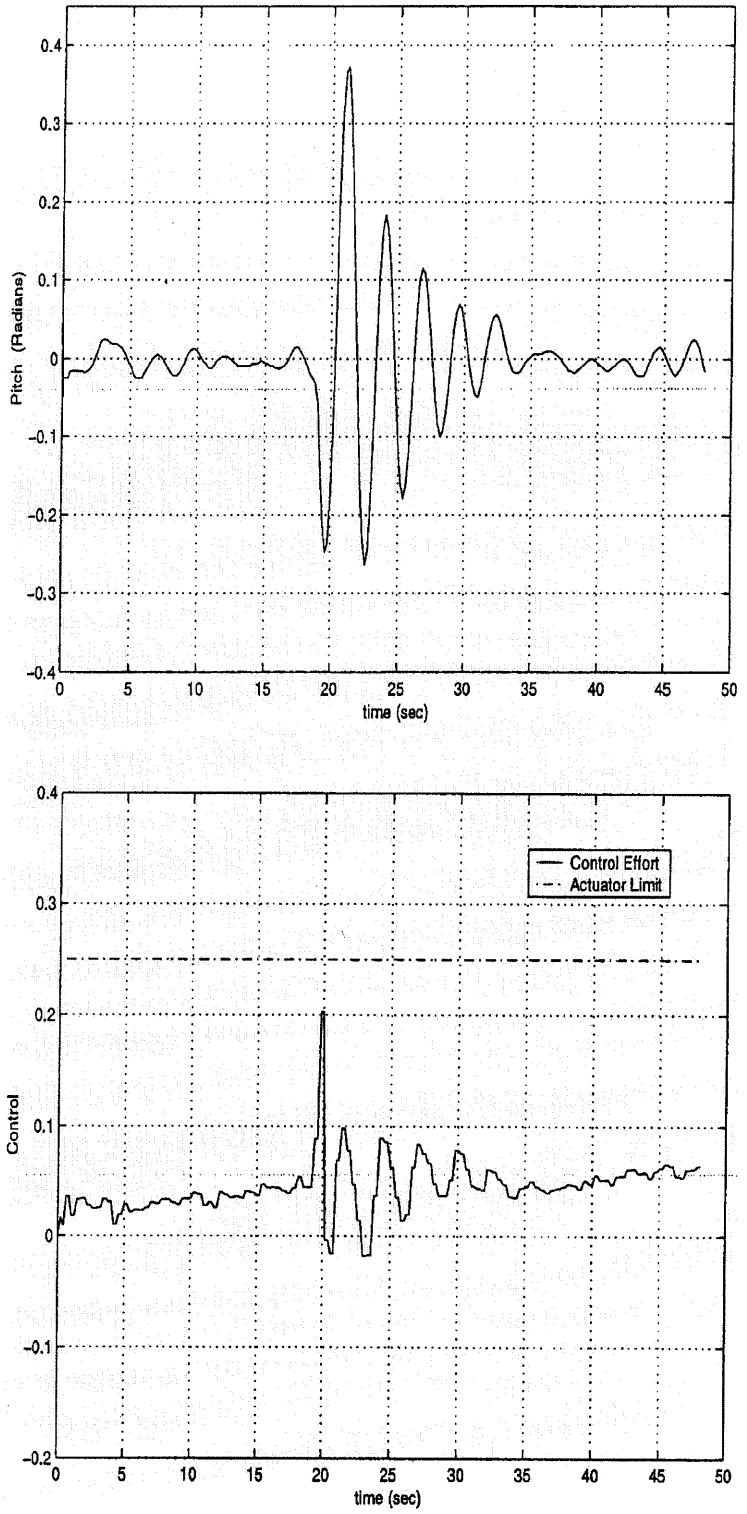


**Fig. 22** Disturbance rejection for $\mathbf{Q} = \mathbf{I}$, $\mathbf{R} = 75$

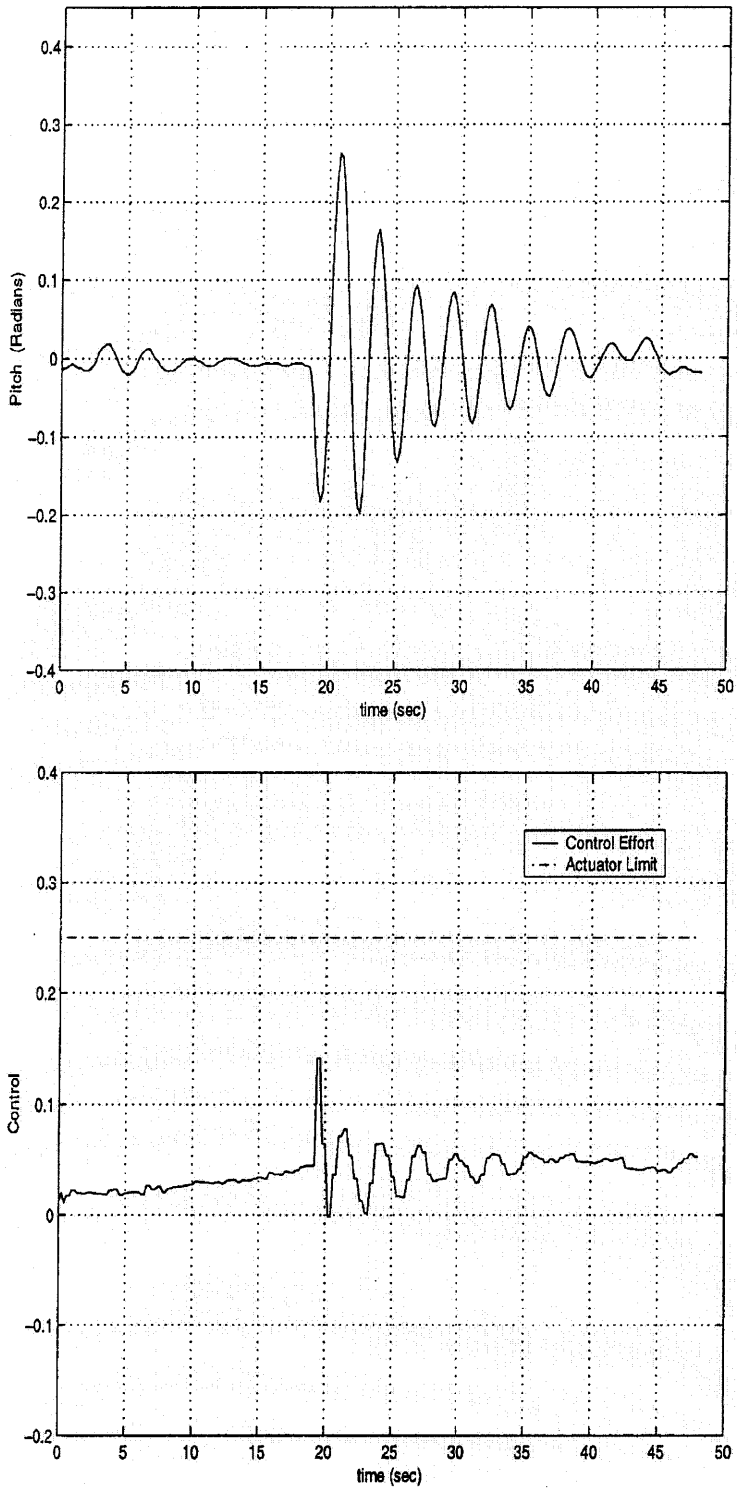


**Fig. 23** Disturbance rejection for $\mathbf{Q} = \mathbf{I}$, $\mathbf{R} = 125$

design specification. The concepts have been verified on a real system, with quite similar results to those achieved in simulations.

Robustness to external disturbance such as wind gust has also been demonstrated, with an acceptable disturbance rejection capability. Note that the successful execution of the controller further corroborates the accuracy of the identified system model.

## ACKNOWLEDGEMENTS

S. M. Ahmad gratefully acknowledges the financial support of the University of Sheffield and the Department of Automatic Control and Systems Engineering.

## REFERENCES

1 **Van Nieuwstadt, M. J.** and **Murray, R. M.** Rapid hover-to-forward-flight transitions for a thrust-vectored aircraft. *Am. Inst. Aeronaut. Astronaut. J. Guidance, Control, and Dynamics*, 1998, **21**, 93–100.

2 **Morris, J. C., Van Nieuwstadt, M. J.** and **Pascale, B.** Identification and control of a model helicopter in hover. In Proceedings of American Control Conference, Baltimore, Maryland, 1994, Vol. 2, pp. 1238–1242.

3 **Werner, H.** and **Meister, T.** Robust control of a laboratory aircraft model via fast output sampling. *Control Engng Practice*, 1999, 7, 305–313.

4 **Sivashankar, N., Kaminer, I.** and **Kuechenmeister, D.** Design, analysis and hardware-in-the-loop simulation of MIMO controller for a VTOL unmanned aerial vehicle using synthesis. In Proceedings of American Control Conference, Baltimore, Maryland, 1994, pp. 2506–2510.

5 **Kaminer, I., Pascoal, A., Hallberg, E.** and **Silvestre, C.** Trajectory tracking for autonomous vehicles: an integrated approach to guidance and control. *Am. Inst. Aeronaut. Astronaut. J. Guidance, Control, and Dynamics*, 1998, **21**, 29–38.

6 **Hallberg, E., Kaminer, I.** and **Pascoal, A.** Development of a flight test system for unmanned air vehicles. *IEEE Control Syst.*, 1999, **19**(1), 55–65.

7 *Company R&D History*, 1997 (Freewing Aerial Robotics, College Station, Texas); www.freewing.com.

8 **Linehan, R. D., Burnham, K. J.** and **James, D. J. G.** 4-Dimensional control of a remotely piloted vehicle. In Proceedings of United Kingdom Automatic Control Conference, Exeter, 1996, pp. 770–775.

9 *Twin Rotor MIMO System. Manual 33-007-0*, 1996 (Feedback Instruments Limited, Sussex).

10 **Ahmad, S. M., Chipperfield, A. J.** and **Tokhi, M. O.** Parametric modelling and dynamic characterization of a two-degree-of-freedom twin rotor multi-input-multi-output system. *Proc. Instn Mech. Engrs, Part G: J. Aerospace Engng*, 2001, **215**(G2), 63–78.

11 **Blight, J. D., Dailey, R. L.** and **Gangsaas, D.** Practical control law design for aircraft using multivariable techniques. In *Advances in Aircraft Flight Control* (Ed. M. B. Tischler), 1996, pp. 231–267.

12 **Ahmad, S. M., Chipperfield, A. J.** and **Tokhi, M. O.** Dynamic modelling and optimal control of a twin rotor MIMO system. In Proceedings of IEEE National Aerospace and Electronics Conference (NAECON'2000), Dayton, Ohio, 10–12 October, pp. 391–398.

13 **Ahmad, S. M., Chipperfield, A. J.** and **Tokhi, M. O.** Dynamic modelling and open loop control of a twin rotor MIMO system. *Proc. Instn Mech. Engrs, Part I: J. Systems and Control Engineering*, 2002, **216**(I6), 477–496.

14 **Ljung, L.** *System Identification Toolbox*, 1991 (The MathWorks Inc., Natick, Massachusetts).

15 **Ljung, L.** *System Identification: Theory for the User*, 1987 (Prentice-Hall International, Englewood Cliffs, New Jersey).

16 **Bryson, A. E.** and **Ho, Y. C.** *Applied Optimal Control*, 1975 (Halsted Press, Washington, DC).

17 **Franklin, G., Powell, J. D.** and **Workman, M.** *Digital Control of Dynamic System*, 1998 (Addison-Wesley, Reading, Massachusetts).

18 **Ahmad, S. M.** Modelling and control of a twin rotor MIMO system. PhD thesis, Department of Automatic Control and Systems Engineering, University of Sheffield, 2001.

19 **Sheperd, C. L.** and **Valavani, L.** Autopilot design for bank-to-turn missiles using LQG/LTR methodology. In Proceedings of American Control Conference, Atlanta, Georgia, 1988, Vol. 1.